REALIZATION OF A THREE-LEVEL NEUTRAL POINT CLAMPED INVERTER USING A NOVEL REGION SELECTION APPROACH OF BUS CLAMPING PWM FOR ELECTRIC VEHICLE APPLICATION

DEBANJAN ROY[1], MADHU SINGH[2]

Keywords: Space vector pulse width modulation (SVPWM); Bus clamping pulse width modulation (BCPWM); Three-level (3L) neutral point clamped (NPC) inverter; Fixed v/f control; Electric vehicle (EV).

This article examines a space vector-based bus clamping control approach for an induction motor driven by a three-level inverter for use in electric vehicles. The suggested controller incorporates a new region identification methodology by combining a basic v/f control with a bus clamping mechanism. In terms of power quality, torque ripple, and capacitor voltage balancing, a comparison to the usual SVPWM approach is made. Previously, lesser attention is paid to space vector-based PWM using a region selection methodology. This strategy is centered upon some algebraic equations. The surprising thing about this sector is that it is identical to all the others. As a result, computation complexity is reduced. This technique applies to any number of levels. The suggested controller's effectiveness is evaluated using the MATLAB/Simulink environment. Transient and steady-state analyses are used to evaluate the entire system's performance. Additionally, the neutral point balance of the 3L NPC inverter is achieved using appropriate switching sequences.

1. INTRODUCTION

Electric vehicles have evolved as an alternate and dependable alternative for the transportation sector because of limited oil resources and increasing air pollution. Selecting an electric motor plays a vital role in any electric propulsion system. Based on various performance parameters presented in [1], different electric motors are graded on a scale of five. Due to low prices, mature technology, and less upkeep, induction and permanent magnet synchronous motors are well-preferred [2,3]. Several traction motors are evaluated in [4] for the same system specifications and dimensions. Permanent magnet synchronous motors (PMSM) are suitable for high power density, reduced loss, and high efficiency. Still, they are restricted because of the high cost and less accessibility of rare-earth magnets [5].

Unlike the current source inverter, the voltage source inverter is favored due to the absence of a line inductor. As a result, VSI has a fast dynamic response. VSIs are classified based on the levels of pole voltage. If pole voltage has a two-level, it is a two-level inverter, whereas pole voltage above two levels represents a multilevel inverter. In the case of a two-level inverter, device-blocking voltage, frequency, switching, and conduction losses are incredibly high. A heat sink dissipates these losses, further increasing the space requirement of the overall system. As a result, the average size of the total unit would increase. As a solution to this problem, multilevel inverters are used. Specifically, it aids in lowering the blocking voltage across each power switch that is less than a two-level inverter [6–9]. This research employs v/f control rather than vector control since it is cheaper and simpler to execute than vector control. An electric vehicle (EV) drive system based on a three-level (3L) neutral point clamped (NPC) inverter driving a squirrel cage induction motor is proposed in [14]. A Sinusoidal pulse width modulation method is used with a constant v/f technique. A study in [10] describes a new space vector modulation algorithm for neutral point balance. In addition, the control scheme uses Mamdani's fuzzy logic controller to boost overall system performance. The developed scheme's performance on motor drive systems is examined in steady-state and transient response modes.

The space vector pulse width modulation (SVPWM) technique is harder to realize for a multilevel inverter. Therefore, working with it necessitates a specific approach. The mapping-oriented method is very familiar and is described in [15]. A reverse mapping concept for a multilevel NPC inverter is presented in [16]. The open loop functioning of the induction motor uses a new technique for region identification for a 3L inverter [11, 12]. In [13], a 3-L inverter with seven segment sequences gets a simpler version of the SVPWM algorithm. A thorough comparison is explored between different switching sequences presented in [12]. Optimal switching sequences are critical in maintaining the neutral point equilibrium in multilevel inverters. It reduces the dependency on an external controller. SVPWM increases dc connection voltage utilization by 15 % over SPWM, making it a safer option for traction applications for researchers. A variety of innovative PWM strategies have been introduced in the literature. A space vector-dependent bus-clamping PWM strategy is referred to in [17], a new PWM technique deduced from the space vector concept. Since fewer switching transitions over an entire cycle, bus-clamping pulse width modulation (BCPWM) has a lower switching loss than traditional SVPWM. During sampling, one step leg is permanently clamped to the positive/negative dc-link terminal.

Torque ripple and stator current ripple are compared in [18–20] between conventional SVPWM, BCPWM, and advanced bus clamping. For an open-loop induction motor, [11] compares the conventional SVPWM and BCPWM techniques in depth. In both steady and transient states, the effectiveness of the suggested controller is investigated. The new area selection approach combined with BCPWM allows closed-loop fixed V/F control. A detailed comparison of continuous switching pulse width modulation (CSPWM) and BCPWM was studied rigorously to validate the algorithms, and analysis has been done for various performance indices.

The paper is divided into four sections. A brief introduction is mentioned at the start. The control scheme for the traction motor is discussed in section two. It discusses the proposed BCPWM algorithm, while section three shows simulation results. Section four concludes the paper with a significant finding.

2. CONTROL STRUCTURE

The control scheme that governs the electric vehicle efficiently is discussed in the current section. It is already shown in the block diagram that a three-phase ac mains FEED power to THE dc-link and the batteries through a

---

[1]Department of Electrical Engineering, Teerthanker Mahaveer University, Moradabad, India, E-mail:debanjanroy88@gmail.com
[2]Department of Electrical Engineering National Institute of Technology, Jamshedpur, India, E-mail: madhu.ee@nitjsr.ac.in

three-phase rectifier. The main aim is to control the traction motor drive using a constant v/f control scheme. It includes a PI-based speed controller that generates slip compensation. Equation 1 represents the slip compensation mathematically. Then it gets added to the measured rotor speed to create an error that can be converted to the frequency with the help of a frequency converter to generate commanded stator voltage.

$$W_{slip} = (W_r^* - W_r)(k_p + \frac{k_i}{s}).\qquad(1)$$

Fig. 1 – Proposed drive system for an induction motor with a three-level inverter.

The Zeigler-Nichols technique tunes K_p and K_i, the PI controller's two key parameters, at the rated load condition. As ki approaches 0, the proportional gain (K_p) gradually increases until the control loop's output oscillates with constant amplitude (K_u). Depending on the type of controller, K_p, and K_i values are determined from Tu (oscillation period) and Ku. Kp and Ki values for any PI controller are 0.45 K_u and 1.25 (K_u/T_u), respectively.

Figure 1 represents the block diagram of the overall system. The v/f control block generates voltage and frequency, which is then sent to the SVPWM pulse-generating block to create pulses. The controlled pulses finally control the three-level NPC inverter to get desired stator voltage to achieve the desired speed.

3. BCPWM TECHNIQUE FOR 3L INVERTER

The BCPWM implementation of a multilevel inverter is more difficult than a two-level inverter. Multilevel inverter topology involves a collection of identical space vectors reflecting redundant state variables. Six big vectors, six medium vectors, twelve short vectors, and three null vectors make up a three-level space vector diagram. These space vectors can result in a hexagonal structure. There are six sectors to it. As seen in Fig. 2, each sector is subdivided into four regions. To find the reference vector, you must first choose a region. The closest three vectors can be used to represent the reference vector. The selection of a region has a major impact on the production of pulses.

High-frequency operation of the multilevel inverters improves the waveform quality. It's possible, though, that this will lead to greater switching losses. Compared to traditional space vector modulation, a given sampling frequency bus clamping PWM technique minimizes switching frequency by 33 %. The three vectors closest to each other can be arranged in various ways to generate clamping sequences. Unfortunately, only a few of these may lead to the lowest possible switching frequency. The following section discusses one such clamping sequence for TYPE II BCPWM.

Fig. 2 – Dimensional representation of space vectors for three-level BCPWM.

Fig. 3 – Representation of regions for sector 1 in the x-y plane.

The clamping sequences must fulfill the following two requirements for the lowest switching frequency.

- Condition 1: Only one switch is allowed during each state change sequence. Only one phase device is permitted to switch during a state transition. Switching from +1 to 1 or *vice versa* is restricted because it simultaneously switches two devices.
- Condition 2: The initial state of any sample is identical to the final state of the previous sample.

The f_r would be maintained constant under high switching frequency. As a result, N will not always be an integer. In certain circumstances, it is impossible to fulfill condition 2 outlined above. However, the switching frequency can be reduced by structuring the sequences so that the violation of condition 2 is minimized. In such situations, switching is permitted only to one of the unclamped phases.

$$F_{sampling\ frequency} = N.\ f_r.\qquad(2)$$

The sequences are structured so that one phase is either clipped to state 1, state 0, or state -1 for each sector or 60°, as seen in Fig. 2. For example, in sector 1, the R phase is clamped to state 1. The technique is analogous to standard SVPWM. Only the sequences and dwell time computation are different in each location. There are four regions in the case of BCPWM, as seen in Fig. 3. The three vectors next to the reference vector are organized so that the needed sequence is obtained when the reference vector is located at region 1.

4. PROPOSED REGION IDENTIFICATION METHOD

This section introduces a novel approach for region selection that relies on algebraic equations to determine the location of the V_{ref}. Fig. 3 illustrates two consecutive sectors (sector 1 and sector 2) and their associated regions. The hexagon's six sections are all symmetrical by nature. As a result, the approach for identifying regions within a sector may readily be extended to different sectors. The zero vectors define the origin of the space vector diagram. A 2-dimensional x-y plane can identify other vectors in that sector, as shown in Fig. 3. The reference vector has an x component (x_1) in phase with the sector's initial vector and a y component perpendicular to the x component. The angle between the starting and reference vectors is denoted by theta. The coordinates of the different space vectors are listed in Table 1.

Table 1
The x-y coordinates for the individual space vectors in sector 1.

Space Vector	Category	Coordinate (X,Y)
V_{25}, V_{26}, V_{27}	null	$(0,0)$
V_1, V_{19}	Short	$\left(\frac{V_{DC}}{3}, 0\right)$
V_{13}	Large	$(2V_{DC}/3, 0)$
V_7	Medium	$\left(\frac{V_{DC}}{2}, \frac{\sqrt{3}V_{DC}}{6}\right)$
V_{14}	Large	$\left(\frac{V_{DC}}{3}, \frac{\sqrt{3}V_{DC}}{3}\right)$
V_2, V_{20}	Short	$\left(\frac{V_{DC}}{6}, \frac{\sqrt{3}V_{DC}}{6}\right)$

This technique focuses on two algebraic equations that govern its operation. Both are representations of a straight line's equation. The first one is derived by joining the coordinates of V_1 and V_2, which are two locations on the graph. Connecting V_1 and V_7 yields a second straight line. Below is a representation of both equations,

$$y_{11} = -\sqrt{3}\left(x - \frac{V_{DC}}{3}\right), \qquad (3)$$

$$y_{22} = \sqrt{3}\left(x - \frac{V_{DC}}{3}\right). \qquad (4)$$

The reference vector V_{ref} is made up of two parts:

$$x_1 = |V_{ref}|\cos\theta \qquad (5)$$
$$y_1 = |V_{ref}|\cos\theta \qquad (6)$$

Inserting the value x1 into eq. (3) and (4), the values for y_{11} and y_{22} may now be determined, as shown below.

$$y_{11} = -\sqrt{3}\left(x_1 - \frac{V_{DC}}{3}\right), \qquad (7)$$

$$y_{22} = \sqrt{3}\left(x_1 - \frac{V_{DC}}{3}\right) \qquad (8)$$

The x-y component of V_{ref} and eq. (6), (7), and (8) are utilized to determine the regions depending on specified criteria. Table 2 lays out the requirements for determining a region's identity. The method is identical to sector 1, except that the x-y coordinate is moved by 60° due to the symmetric structure of all sectors.

Table 2
Conditions for region selection in any sector.

Region	Condition
1	$0 < x_1 \le V_{DC}/6$ and $0 \le \theta \le 60°$ or $V_{DC}/6 < x_1$ and $y_1 \le y_{11}$
2	$V_{DC}/6 < x_1$ and $y_{11} < y_1 \le \sqrt{3}V_{DC}/6$ or $V_{DC}/2 > x_1$ and $y_{22} < y_1 \le \sqrt{3}V_{DC}/6$
3	$V_{DC}/2 < x_1$ and $y_1 \le y_{22}$
	or $V_{DC}/2 < x_1$ and $0 \le \theta \le 30°$
4	If the first three requirements aren't met, move on to region 4.

5. SWITCHING SEQUENCES AND CALCULATIONS OF DWELL TIME

The possible sequences for all the regions in a sector are presented in Table 3.

Table 3
The possible sequences for all the regions in a sector.

Region	Vector Sequence	Clamped Phase
1	$V_1 \Leftrightarrow V_2 \Leftrightarrow V_{25}$ (100) (110) (111)	+R
2	$V_2 \Leftrightarrow V_1 \Leftrightarrow V_7$ (110) (100) (10-1)	+R
3	$V_1 \Leftrightarrow V_7 \Leftrightarrow V_{13}$ (100) (10-1) (1-1-1)	+R
4	$V_2 \Leftrightarrow V_{14} \Leftrightarrow V_7$ (110) (11-1) (10-1)	+R

The hexagon plays a vital role in determining the dwelling times in each sector. The three-level space vector diagram has six symmetrical sectors, each with four regions. Let's assume that a reference vector is placed in region 2. The nearest three vectors, basically the vertex of the specific triangle, need to be located. In this case, they are V_1, V_7, and V_2. Now we can find the following vol-sec balance equation,

$$V_1 * T_a + V_7 * T_b + V_2 * T_c = V_{ref} * T_s. \qquad (8)$$

The dwell times for the space vector V_1, V_7, and V_2 of region 2 are T_a, T_b, and T_c, respectively. It is the length of time that the space vectors are active. By combining the values of V_1, V_7, and V_2 of together, we get

$$\frac{V_d}{3} * T_a + \frac{V_d}{3}(\cos 60° + \sin 60°) * T_b +$$
$$\frac{\sqrt{3}V_d}{3}\left(\cos 30° + \sin 30°\right) * T_c = V_{ref} * T_s \qquad (9)$$

$$T_a + T_b + T_c = T_s \qquad (10)$$

When we derive the real and imaginary parts of eq. (9), the required dwell times for the voltage vectors may be calculated for region 2. Likewise, as indicated in Table 4, dwell times for various regions are determined. Modulation Index (MI) $= \sqrt{3} * \left(V_{ref}/V_{DC}\right)$.

Table 4
Switching times for sector 1

Region	Space Vectors	Dwell Time
1	V_1, V_{19}	$T_b = T_S\{2 - 2m\sin(\pi/3 + \theta)\}$
	V_{26}	$T_c = T_S\{2m\sin\theta\}$
	V_{20}	$T_c = T_S\{2m\sin(\pi/3 - \theta) - 1\}$
2	V_1, V_{19}	$T_a = T_S\{1 - 2m\sin\theta\}$
	V_7	$T_b = T_S\{2m\sin(\pi/3 + \theta) - 1\}$
	V_{20}	$T_c = T_S\{1 - 2m\sin(\pi/3 - \theta)\}$
3	V_1, V_{19}	$T_b = T_S\{2m\sin(\pi/3 - \theta)\}$
	V_7	$T_c = T_S\{1 - 2m\sin(\pi/3 + \theta)\}$
	V_{13}	$T_b = 2T_S m\sin\theta$
4	V_{14}	$T_b = T_S\{2m\sin\theta - 1\}$
	V_7	$T_b = T_S\{2m\sin(\pi/3 - \theta)\}$
	V_2, V_{20}	$T_b = T_S\{2 - 2m\sin(\pi/3 + \theta)\}$
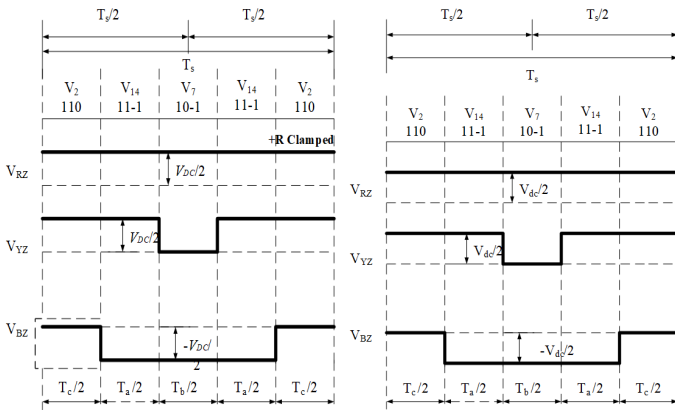
Fig. 4 –Five segment switching sequence for region 1
(R phase clamped to +ve)

6. SYSTEM DESCRIPTION

The system is examined under the following conditions: dc bus voltage, V_{dc}= 353 V; rated power = 4 kW; nominal speed = 1430 r.p.m; Rs =1.405 Ω, R_r =1.395 Ω, L_m = 0.1722 H and L_{ls} = L_{lr}= 0.005839 H f_{sw} (switching frequency) = 5 kHz.

7. SIMULATION RESULTS

To conclude this part, a detailed analysis of the BCPWM algorithm is performed with the help of simulation. It has been compared to a traditional SVPWM scheme at the same switching frequency of 5 kHz. The results depict the performance of the overall control system. 3L NPC inverter's neutral point balancing problem is also examined for the PWM approaches. The transient and steady-state analysis has been conducted. It has three main sections: one being speed response, and the other two being torque response and steady-state response. It is possible to distinguish speed response (a change in speed) from torque response (a change in torque).

6.1. SPEED RESPONSE

To start the system, we use a reference speed of 700 revolutions per minute (RPM) and a reference torque of 10 Nm. Reference torque is kept constant at 10 Nm at t = 4 s. The details are depicted in Fig. 5.
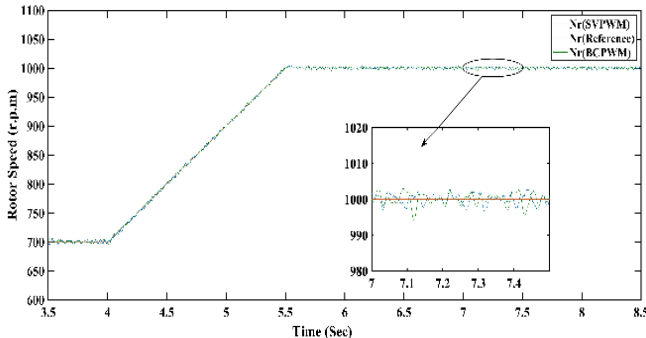
Fig. 5 – Rotor speed.

Reference speed increases from 700 to 1000 r.p.m at t = 4 s while keeping reference torque constant at 10 Nm. System movement is seen in Fig. 5 and Fig. 6 with the speed change. The noteworthy feature is that the rotor speed consistently and reliably matches its reference value, which shows that the recommended BCPWM algorithm is successful.

Additionally, Fig. 7 shows the simulation results of the proposed drive system, which employs SVPWM, operating at the same switching frequency. It can be observed from Fig. 6(a)

and Fig. 7(a) that the electromagnetic torque ripple decreases to 2.34 Nm in the case of BCPWM.
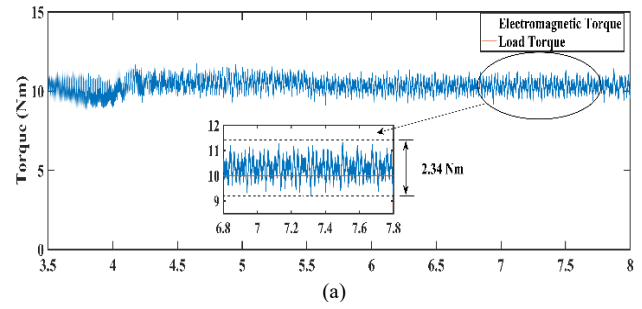
(a)
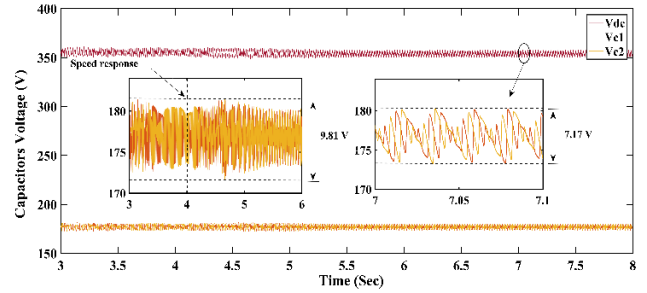
(b)

Fig. 6 – Speed response using BCPWM: (a) electromagnetic torque, (b) capacitors voltage.
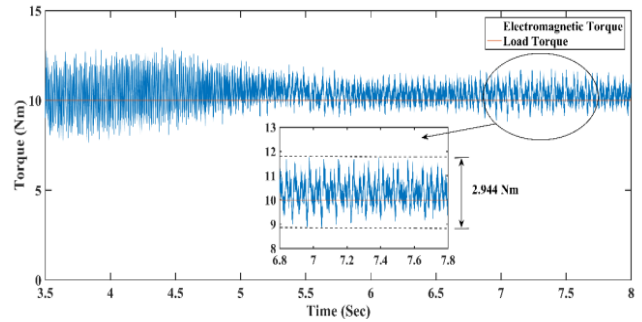
(a)
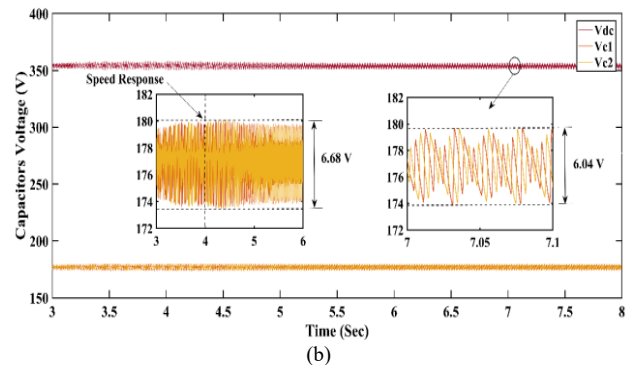
(b)

Fig. 7 – Speed response using SVPWM: (a) electromagnetic torque, (b) capacitors voltage.

In addition, neutral point voltage is also examined for the NPC inverter. The upper capacitor and lower capacitor voltages are represented by V_{c1} and V_{c2}, respectively. The voltage ripple of the capacitors is seen throughout the speed response depicted in Fig. 7(b), which talks about the voltage ripple during the transient and steady state, reaching 6.68 V and 6.04 V, respectively, for SVPWM. Figure 7,b presents the familiar investigation for the BCPWM scheme; values are 9.81 V and 7.17 V, respectively. Considering the effect of BCPWM, torque ripple is reduced; however, capacitor ripple is increased. The algorithm works satisfactorily to keep the ripple of dc bus voltage below 5 % of the overall dc link voltage.

6.1.2. TORQUE RESPONSE

Torque is raised from 10 to 15 nm at $t = 9$ s while maintaining a constant speed of 1000 r.p.m. Figure 8 illustrates the rotor speed behavior in response to torque for SVPWM and BCPWM. Svpwm makes transitions faster than bcpwm and stabilizes the speed within 0.3 s.
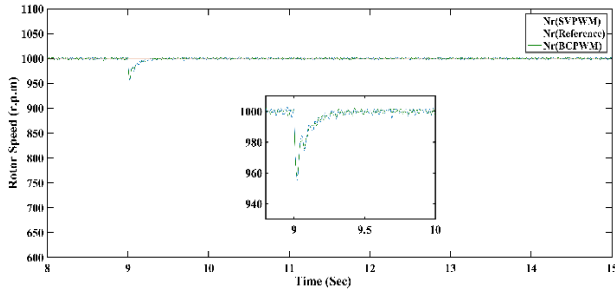
Fig. 8 – Rotor speed
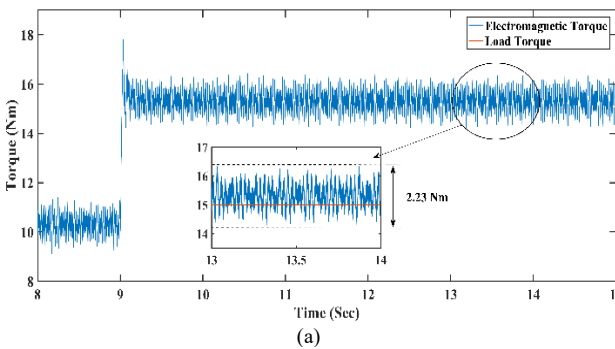
(a)
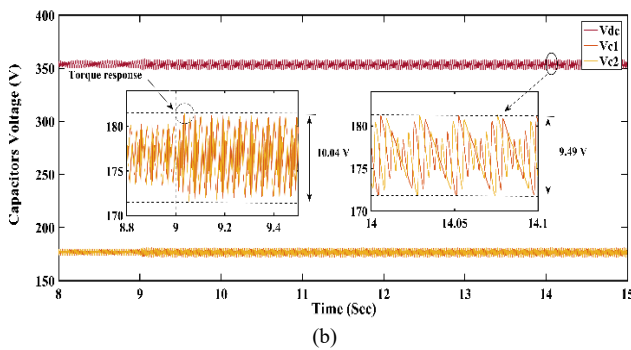
(b)

Fig. 9 –Torque response using BCPWM: (a) rotor speed,
(b) electromagnetic torque, (c) capacitors voltage.
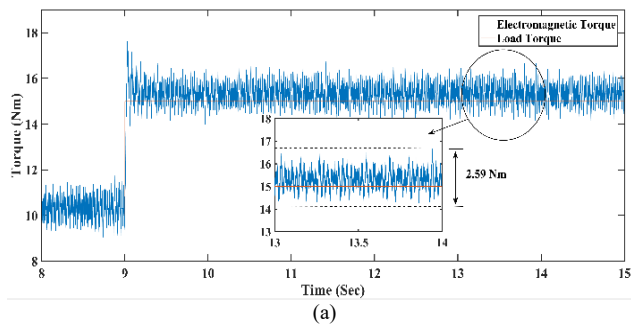
(a)
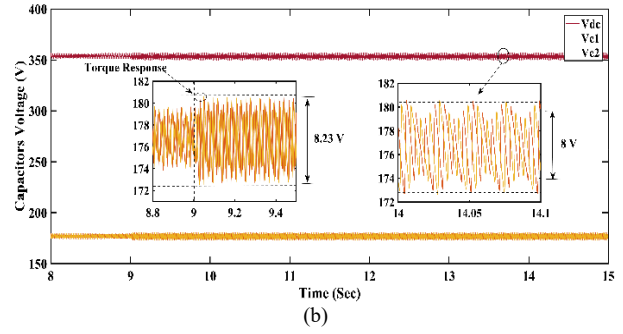
(b)

Fig. 10 – Torque response using SVPWM: (a) electromagnetic torque, (b) capacitors voltage.

Figure 9 (a) depicts the system's electromagnetic torque behavior. Under the steady-state condition, it is observed again that the ripple in electromagnetic torque is decreased to 2.23 Nm when SVPWM is used. In Fig. 9,b, at $t = 9$ s and in the steady-state, capacitor voltage ripples are explored. Again, as seen in Fig. 9, 10 the BCPWM approach increases the ripple in the capacitor voltage.

6.1.3. STEADY-STATE RESPONSE

The rotor revolves at 1000 rpm in a steady state. Figure 11,a and Fig. 12,a illustrate the stator current and voltage for BCPWM, respectively. The stator current is analyzed using FFT analysis in Fig. 11. (b). Figure 12,b determines the FFT analysis of line voltage at 35.7 Hz. The switching frequency of the inverter is kept at 5 KHz. The harmonics appear as sidebands centered around the switching frequency and its multiples, for example, around 5 kHz, 10 kHz, 15 kHz, etc. The line voltages of the inverter supplied to the stator are seen in Fig. 11 (a).
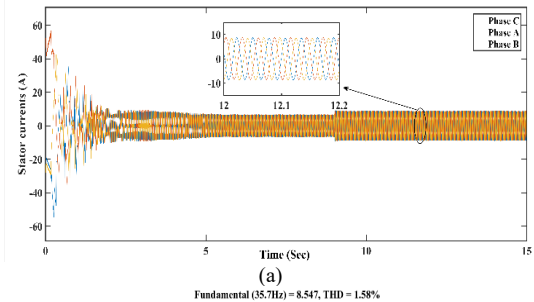
(a)
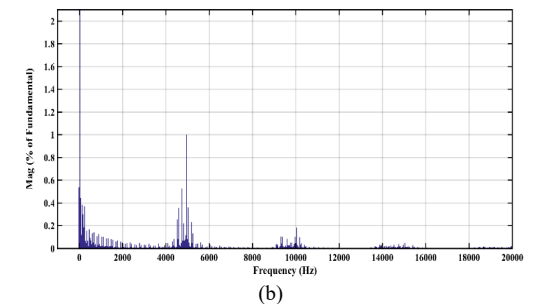
(b)

Fig. 11 – Simulation results for BCPWM (a) stator currents,
(b) FFT analysis of stator current.
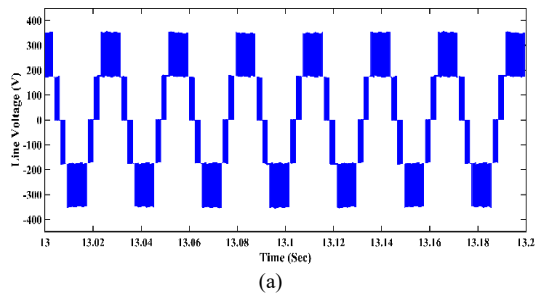
(a)
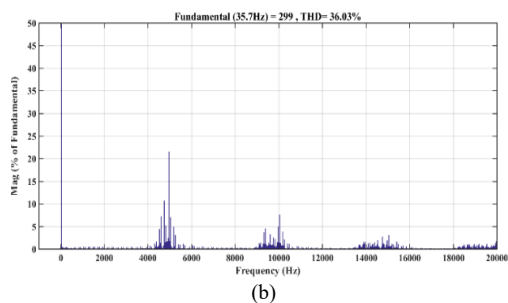
Fig. 12 – Simulation results for BCPWM (a) Line voltage,
(b) FFT analysis of line voltage.

The stator current and voltage for SVPWM are depicted
in Fig. 13. (a) and Fig. 14. (a). Fig. 13(b) shows a
measurement of the stator current. Figure 14(b) shows the
line voltage's FFT analysis at 35.7 Hz. The inverter's
switching frequency is kept constant at 5 kHz.
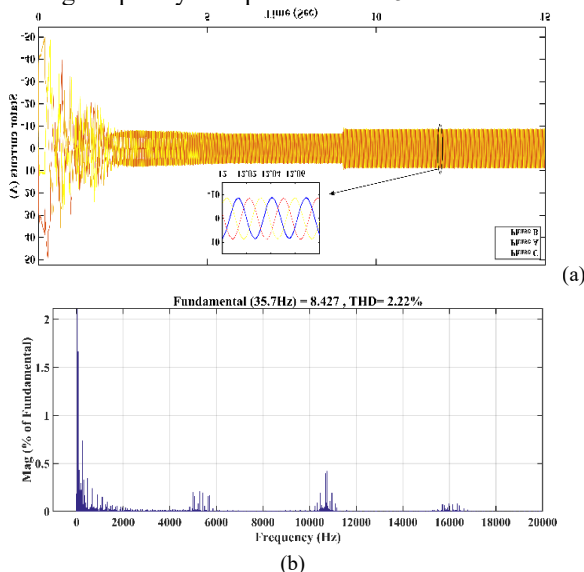
Fig. 13 – Simulation results for SVPWM (a) 3-phase stator
currents, (b) FFT analysis of phase A current.

In Table 5, several performance parameters are compared
in great depth. The %THD of stator current is reduced by
28.82 % using BCPWM.

Table 5

Comparison of SVPWM and BCPWM at 5 kHz switching frequency.

Performance Parameters	Space Vector PWM	Bus Clamping PWM
%THD of stator Current	2.22 %	1.58 %
Peak value fundamental stator Current	8.427 A	8.547 A
%THD of stator voltage	35.54 %	36.06 %
Peak value of fundamental stator voltage	301.5 V	299 V

(a)
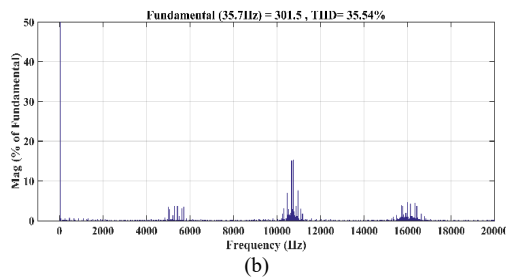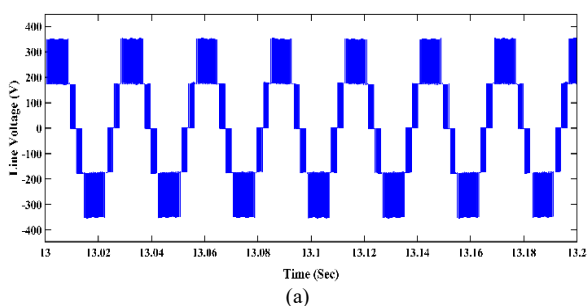
Fig. 14 – Simulation results for SVPWM (a) line voltage,
(b) FFT analysis of line voltage.

Several harmonic frequencies centered around the
switching frequency and its multiples, such as 5, 10, 15, *etc*.
Figure 14,a shows the inverter's line voltage going to the
stator of the induction motor.

8. CONCLUSION

An all-new approach to region selection of a 3-level
BCPWM for electric vehicle applications has been
demonstrated in this paper. The main objective is to develop
a simple, easy-to-implement, and effective region selection
approach for multilevel inverters where the inverter has a
greater number of states. In MATLAB/Simulink
environment, a 4-kW induction motor is used as a model for
a traction motor. The results of the system's speed and torque
response supported the efficacy of the method described. The
capacitor voltage ripples were kept within an acceptable
range under a steady state. The usefulness of the proposed
technique has also been presented through the harmonic
analysis of stator voltage and current.

Furthermore, the traditional SVM methodology is
compared with the BCPWM for the three-level inverter. The
results justify certain improvements in terms of %THD of
stator current and torque ripple. Finally, the practical
execution of this suggested work will be a complicated
technical feat to accomplish in the future.

Received on 30 December 2021

REFERENCES

1. S.J. Rind, Y. Ren, Y. Hu, J. Wang, L. Jiang, *Configurations and control of traction 4 motors for electric vehicles: a review*, Chinese Journal of Electrical Engineering, **3**, *3*, pp. 1–17 (2017).
2. S.T. Varghese, K.R. Rajagopa, *Economic and efficient induction motor controller for electric vehicle using improved scalar algorithm*, 1st IEEE International Conference on Power Electronics, Intelligent Control, and Energy Systems, 1-17 (2016).
3. N. Hashernnia, B. Asaei, *Comparative study of using different electric motors in the electric vehicles*, 18th International Conference on Electrical Machines, Vilamoura, Portugal, 1-5, Sept. 2008.
4. G. Pellegrino, A. Vagati, B. Boazzo, P. Guglielmi, *Comparison of induction and PM synchronous motor drives for EV application including design examples*, IEEE Transactions on Industry Applications, **48**, *6*, pp. 2322–2332 (2012).
5. P. Xue, J. Lin, *Discussion on the rare earth resources and its development potential of Inner Mongolia of China*, Proc. ICMREE, Shanghai, China, pp. 9–12 (2011).
6. L. Clotea, A. Forcos, C. Marinescu, M. Georgescu, *Power loss analysis of two-level and three-level neutral point clamped inverters for a wind pump storage system*, Proc. on IEEE 12th Int. Conf. on Optimization of Electrical and Electronic Equipment, Brasov, Romania, pp. 1174–1179 (2010).
7. R. Macke, *Multilevel NPC inverter for low-voltage applications,* Proc. IEEE 14th European Conf. on Power Electronics Applications, Birmingham, UK, 1–10 (2011).
8. Z. Chen, L. Yuan, Z. Zhao, *Power losses in two and three-level three-phase photovoltaic inverters equipped with IGBT's*, Proc. IEEE 15th

Int. Conf. on Electrical Machines and Systems, Sapporo, Japan, 1-6 (2012).

9. R. Teichmann, S. Bernet, *A comparison of three-level converter versus two-level converters for low-voltage drives, traction, and utility applications,* IEEE Trans. on Industry Applications, **41**, *3*, pp. 855–865 (2005).

10. R.T. Nathenas, G. Adamidis, *A new approach for SVPWM of a three-level inverter-induction motor fed-neutral point balancing algorithm*, Simulation Modeling Practice and Theory, Elsevier, **29**, pp. 117 (2012).

11. D Roy, M Singh, T Roy, *A novel approach for space vector based PWM algorithm for diode clamped three-level VSI fed induction motor drive*, Int. Journal of Power Electronics and Drive Systems, **8**, *4*, pp. 1534–1547 (2017).

12. D. Roy, T. Roy, *A new technique to implement conventional as well as advanced Pulse Width Modulation techniques for multi-level inverter,* IEEE 6th India International Conference on Power Electronics (IICPE), Kurukshetra, India, 1-6, Aug. 2014.

13. D. Roy, M. Singh, *A simplified space vector pulse width modulation for three-phase three-level diode clamped inverter*, 1st IEEE Int. Conf. on Smart grids, Power and Advanced Control Engineering (ICSPACE), Bangalore, India, 226-230 (2017).

14. M.A. Gonzalez, M.F. Escalante, *Traction system for an EV based on induction motor and 3-level NPC inverter multilevel converters*, 12th IEEE International Power Electronics Congress, San Luis Potosi, Mexico, pp. 2873–77 (2010).

15. A.S. Mohamed, A. Gopinath, M.R. Baiju, *A simple space vector PWM generation scheme for any general n-level inverter*, IEEE Transactions on Industrial Electronics, **56**, pp. 1649–1656 (2009).

16. N. Susheela, P. Satish Kumar, S.K. Sharma, *Generalized algorithm of reverse mapping based SVPWM strategy for diode clamped multilevel inverters*, IEEE Transactions on Industrial Applications, **54**, *3*, pp. 2425–2437 (2018).

17. A. R. Beig, Ranganathan V.T., Space vector-based bus clamped PWM algorithms for three-level inverters: implementation, performance analysis, and application considerations, *Applied Power Electronics Conference and Exposition (APEC) Eighteenth Annual IEEE*, **1**, pp. 569–575 (2003).

18. V.S.S.P.K. Hari, G. Narayanan, *Theoretical and experimental evaluation of pulsating torque produced by induction motor drives controlled with advanced bus-clamping pulse-width modulation*, IEEE Transactions on Industrial Electronics, **63**, *3*, pp. 1404–1413 (2016).

19. E. Benyoussef, S. Barkat, *Three-level direct torque control based on balancing strategy of five-phase induction machine*, Rev. Roum. Sci. Techn. – Électrotechn. et Énerg., **67**, *2*, pp. 93–98 (2022).

20. S.-A. Touil, N. Boudjerda, A. Boubakir, K. El Khamlichi Drissi, *Closed loop discontinuous pulse width modulation control used in inverter grid-connected photovoltaic system for reduced switching losses*, Rev. Roum. Sci. Techn. – Électrotechn. et Énerg., **64**, *4*, pp. 357–363 (2022).